

Inelastic scattering in a monolayer graphene sheet: A weak-localization study

Dong-Keun Ki, Dongchan Jeong, Jae-Hyun Choi, and Hu-Jong Lee*

Department of Physics, Pohang University of Science and Technology, Pohang 790-784, Republic of Korea

Kee-Su Park

Department of Physics, Pusan National University, Busan 609-735, Republic of Korea

(Received 19 June 2008; published 12 September 2008)

Charge carriers in a graphene sheet, a single layer of graphite, exhibit distinct characteristics from those in other two-dimensional electronic systems because of their chiral nature. In this paper, we focus on the observation of weak localization in a graphene sheet exfoliated from a piece of natural graphite and nanopatterned into a Hall-bar geometry. Much stronger chiral-symmetry-breaking elastic intervalley scattering in our graphene sheet restores the conventional weak localization. The resulting carrier density and temperature dependence of the phase coherence length reveal that the electron-electron interaction including a direct Coulomb interaction is the main inelastic-scattering factor while electron-hole puddles enhance the inelastic scattering near the Dirac point.

DOI: [10.1103/PhysRevB.78.125409](https://doi.org/10.1103/PhysRevB.78.125409)

PACS number(s): 72.15.Rn, 73.20.Fz, 73.43.Qt, 73.23.-b

I. INTRODUCTION

Since charge carriers in graphene, a single layer of graphite, have a unique chiral nature,¹ the interference of carriers²⁻⁸ is not only sensitive to breaking of the phase coherence represented by the characteristic scattering rate of τ_ϕ^{-1} but also sensitive to breaking of the chiral symmetry.^{9,10} In particular, in the case of weak localization¹¹ (WL) in graphene, the random gauge field generated at surface ripples¹² is believed to suppress the WL effect² while conventional WL (Refs. 3 and 4) and anti-WL (Ref. 5) have also been reported. In general, WL of charge carriers takes place as they are coherently backscattered¹¹ [Fig. 1(b)]. Charge carriers in graphene, however, accumulate the Berry phase π if the chiral symmetry is conserved during the coherent backscattering along a gray-circle path on the surface of a cone-shape dispersion relation in Fig. 1(c).^{9,10} Thus, as long as the chiral symmetry is conserved, anti-WL is expected to be revealed in graphene due to the sign change of the quantum interference correction to the conductivity.^{5,9,10} But, this anti-WL itself is suppressed by the trigonal warping, which breaks the time-reversal symmetry in a valley at the rate of τ_w^{-1} , and also by the chiral-symmetry-breaking elastic intravalley scattering,^{9,10} as denoted by the dotted arrow in Fig. 1(c) at the rate of τ_z^{-1} .

On the other hand, the conventional character of WL can be recovered by the elastic intervalley scattering^{3,9,10} at the characteristic rate of τ_i^{-1} [denoted by the solid arrow in Fig. 1(c)]. Both the intravalley and the intervalley scatterings are possible only when the chiral symmetry is broken by surface ripples, atomic-sized defects, boundaries, etc.⁹ Thus, WL in graphene strongly depends on such detailed sample conditions. This can be the reason for some contradictory outcomes in previous observations.²⁻⁵

We report WL in a Hall-bar-patterned 1- μm -wide graphene sheet [denoted by a white line in Fig. 1(a)] with much stronger elastic intervalley scattering ($\tau_i^{-1} \gg \tau_\phi^{-1}$) than in previous works.^{2,3,5} Detailed examination of the gate-voltage and temperature dependencies of the phase coher-

ence length (L_ϕ) in this study indicates that the electron-electron interaction^{13,14} is the main inelastic-scattering factor at temperatures of our measurement range (below ~ 20 K) (Refs. 2 and 3) while electron-hole puddles¹⁵ enhance the inelastic scattering near the Dirac point (DP).^{3,7}

II. SAMPLE PREPARATION AND MEASUREMENTS

A monolayer graphene sheet used in this study was mechanically exfoliated¹ from a natural graphite piece onto a highly doped silicon substrate covered with a 300-nm-thick SiO_2 layer. After electric contacts were made by conven-

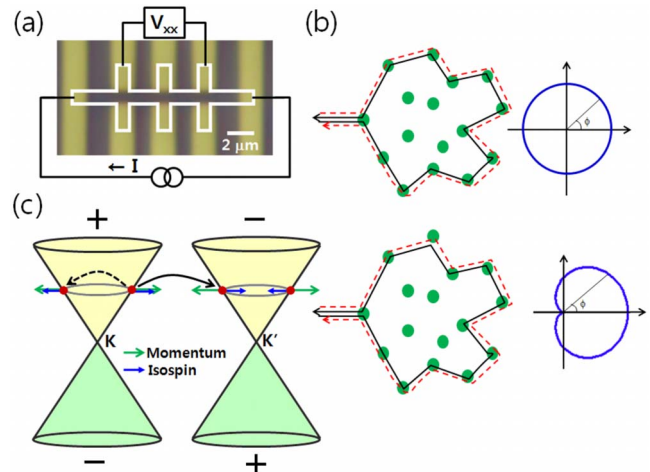


FIG. 1. (Color online) (a) Sample geometry and measurement configuration. The boundary of our graphene sheet is denoted by a white line. (b) Upper set: time-reversal closed paths contributing to WL in a normal electronic system with an isotropic scattering probability (shown on the right). Lower set: similar time-reversal closed paths in graphene with an anisotropic scattering probability (shown on the right). (c) A cone-shape energy dispersion relation of graphene. There are two different K points (valleys) with different chiralities (denoted by \pm). The dotted and solid arrows represent the intravalley and the intervalley scatterings, respectively.

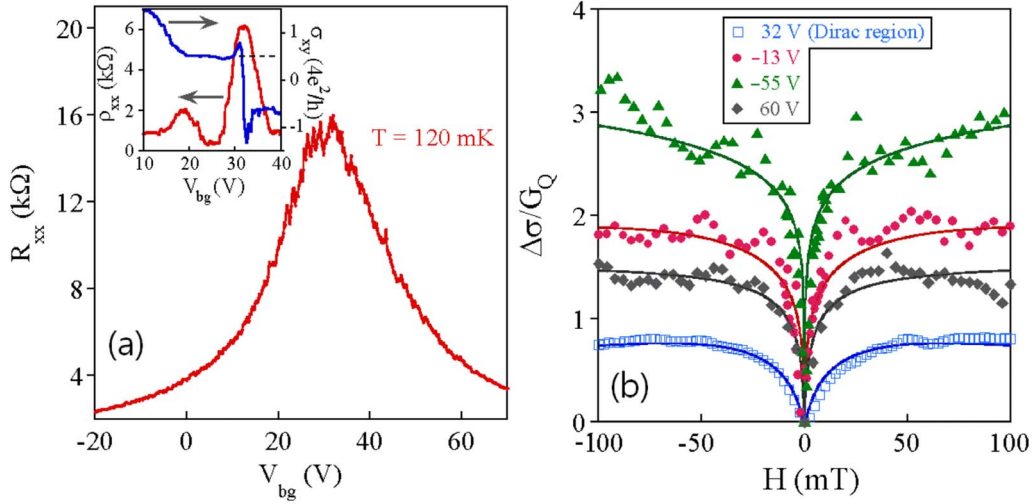


FIG. 2. (Color online) (a) The back-gate-voltage dependence of the longitudinal sample resistance. The mobility (μ) of the sample is ~ 4000 $\text{cm}^2/\text{V s}$ outside the Dirac region. Inset: the half-integer quantum Hall effect measured in 9 T and at 120 mK confirms that our graphene sheet is single layered. (b) Correction of the magnetoconductivity for various gate voltages ($G_Q = e^2/h$). The carrier density can be estimated with a relation $n(\text{in cm}^{-2}) = 7 \times 10^{10} [V_{bg}(\text{in V}) - 32]$ with the positive (negative) value for electrons (holes). Dots and lines represent experimental data and best fits, respectively.

tional e -beam lithography and subsequent e -beam evaporation of Cr (5 nm) and Au (70 nm), a Hall-bar geometry was defined by oxygen plasma etching (for 90 s at 50 W) with a negative e -beam-resist stencil patterned by e -beam lithography [denoted by a white line in Fig. 1(a)].

Measurements were made by using a dilution fridge (Oxford model Kelvinox) with the base temperature as low as 120 mK. Each lead contact showed resistance of ~ 400 Ω with a negligible temperature dependence. The longitudinal sample resistance vs the back-gate voltage, as shown in Fig. 2(a), reveals the charge-neutrality DP at $V_{bg} = 32$ V. In addition, the half-integer quantum Hall effect¹ in a field of 9 T [the inset of Fig. 2(a)] confirms the single layeredness of our graphene sheet. Because of the mesoscopic size of the sample (1×6 μm^2), the universal conductance fluctuation (UCF) was also observed just like in the previous studies^{2-4,6,7} (not shown). Thus, following Ref. 3, the fluctuation in the magnetoconductivity (MC) was averaged out over a 2 V range of back-gate voltage to get the conductivity correction as $\Delta\sigma(V_{bg}, B) = [\sigma(V, B) - \sigma(V, 0)]_{(V_{bg}-1V \leq V \leq V_{bg}+1V)}$. The resultant data are shown as dots in Fig. 2(b).

III. RESULTS AND DISCUSSION

For analysis, we use the expression for the WL-induced conductivity correction as theoretically suggested with three parameters¹⁰ (L_ϕ , L_i , and L_*)

$$\Delta\sigma = \frac{e^2}{\pi h} \times \left[F\left(\frac{8\pi B}{\Phi_0 L_\phi^{-2}}\right) - F\left(\frac{8\pi B}{\Phi_0 \{L_\phi^{-2} + 2L_i^{-2}\}}\right) - 2F\left(\frac{8\pi B}{\Phi_0 \{L_\phi^{-2} + L_i^{-2} + L_*^{-2}\}}\right) \right], \quad (1)$$

where $F(z) = \ln z + \psi(0.5 + z^{-1})$, [$\psi(x)$, the digamma function;

$\Phi_0 (= h/e)$, flux quantum]. L_ϕ and L_i stand for the phase coherence length and the elastic intervalley scattering length with the relation $L_{\phi,i} = \sqrt{D\tau_{\phi,i}}$ (D is the diffusion constant of the graphene sheet), respectively, while L_* is defined by the combination of τ_z^{-1} and τ_w^{-1} as $L_* = \sqrt{D\tau_*}$ and $\tau_*^{-1} = \tau_z^{-1} + \tau_w^{-1}$.

Figure 2(b) shows the differential MC data taken at the base temperature of 120 mK for the selected gate voltages, which show the positive MC, i.e., the conventional character of WL. Best fits of the data to Eq. (1) are shown as solid lines in Fig. 2(b). The conductivity dip at zero magnetic field gets deeper as the gate voltage is shifted from the DP, which indicates an increase in L_ϕ with increasing the carrier density n . Although similar behavior was also observed previously³ at a few gate voltages, no systematic studies on this effect were pursued.⁶ The best-fit values for the parameters L_ϕ , L_i , and L_* , determined from the plot in Fig. 2(b), are given in Fig. 3(a), which clearly show that L_ϕ becomes longer as the carrier density increases. However, the characteristic lengths for the elastic intervalley scattering (L_i) and other kinds of elastic scattering (L_*) remain almost unchanged at values much smaller than L_ϕ at all gate voltages.

Since only the first term in Eq. (1) gives a positive MC, the conventional character of WL becomes most prominent when both the intravalley and the intervalley scatterings are strong so that $L_\phi \gg L_i \gtrsim L_*$, which is the case of this study. In comparison, the previous study by Morozov *et al.*² corresponds to the negligible intervalley scattering as $L_i \gg L_\phi \gg L_*$ while $L_\phi \sim L_i \gg L_*$ for the majority of the samples in the work by Tikhonenko *et al.*³ A high intervalley scattering rate was also observed in the narrowest sample of the work of Ref. 3, which was caused by the boundary scattering. By contrast, the strong elastic intervalley scattering in our study takes place in a much wider graphene sheet, where the boundary scattering is supposedly negligible. Thus, we

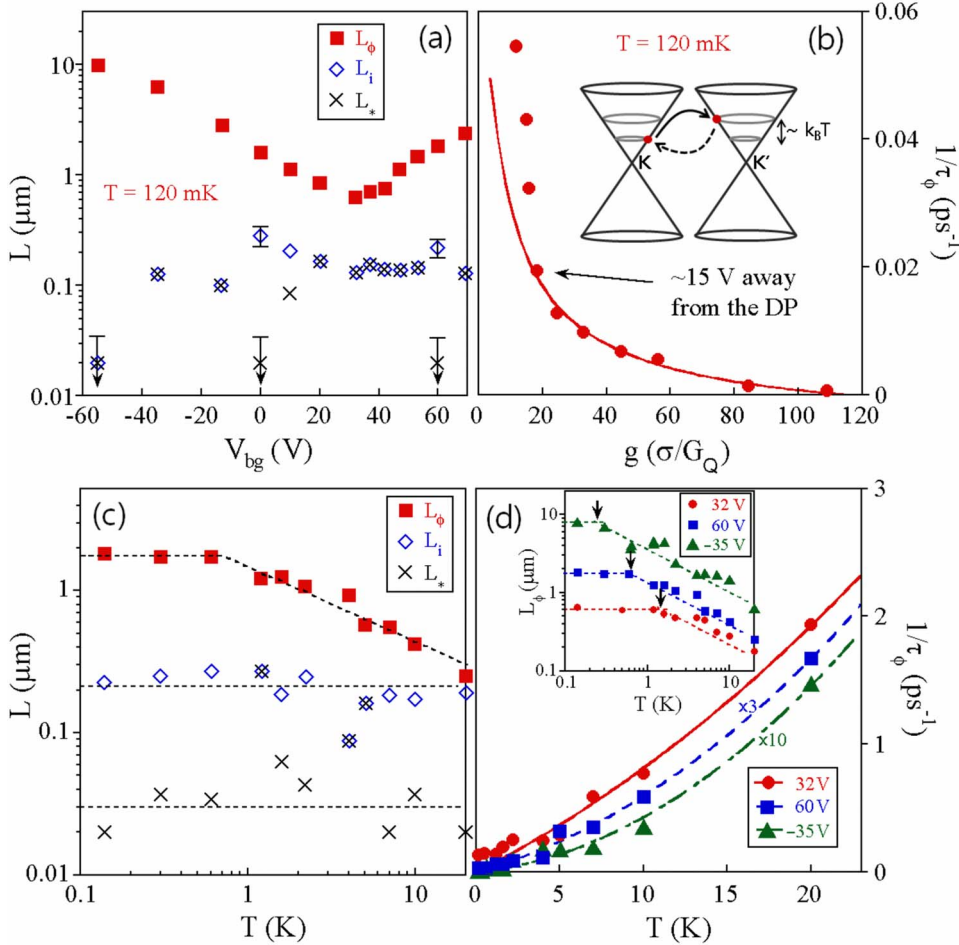


FIG. 3. (Color online) (a) Best-fit values of the characteristic lengths as a function of gate voltage at the base temperature of 120 mK. As denoted by arrows, the lower bounds of the error bars of L_* for a few V_{bg} go as low as ~ 1 nm, which are not physical and are considered to arise from the uncertainty involved in fitting to the particular functional form of Eq. (1) as discussed in Ref. 3. (b) Inelastic scattering rate as a function of conductance g at the base temperature, 120 mK. The line is a best fit to the first term in Eq. (2). (c) Temperature dependence of the characteristic lengths at a dense-electron region ($V_{bg} \sim 60$ V). Dotted lines are guides to the eyes. (d) Inelastic scattering rates at different gate voltages as a function of temperature. The values of τ_ϕ^{-1} for $V_{bg}=60$ V (-35 V) is multiplied by a factor of three (ten) for clarity of the temperature dependence. Lines are best fits to Eq. (2). Inset: Temperature dependence of L_ϕ . Dotted lines are guide to the eyes and the arrows indicate the saturation temperature (T_{sat}).

believe that the strong elastic intervalley scattering in our system was mainly caused by atomically sharp defects, which are known to make both the intervalley and the intravalley scatterings strong.³ The sharp defects in our sample may have resulted from the strong coupling between the graphene sheet and the Si substrate or any mechanical defects introduced during the exfoliation process.

As the conventional WL effect is restored by the high elastic intervalley scattering rate in our graphene sheet, a convenient condition is provided to examine the *inelastic-scattering* characteristics in graphene. At low temperatures, the electron-electron interaction^{13,14} is considered to be the major source of the inelastic scattering in graphene.^{2,3,16} The inelastic scattering by the electron-electron interaction can be divided into two terms: the direct Coulomb interaction (τ_{ee}^{-1}) among electrons and the interaction of an electron with the fluctuating electromagnetic field generated by the noisy movement of neighboring electrons (Nyquist scattering, τ_N^{-1}).^{13,14} Both interactions depend on the carrier density along with the screening by neighboring charge carriers, which was proven a decade ago in a GaAs/AlGaAs heterojunction two-dimensional electron-gas (2DEG) system.¹⁴ In graphene, different from 2DEG, $E_F \propto k_F \sim \sqrt{n}$ and the Fermi velocity v_F is independent of n (Ref. 1) so that the interaction depends on the carrier density as

$$\begin{aligned}
 1/\tau_\phi &\propto 1/\tau_N + 1/\tau_{ee} + \text{const} \\
 &\propto ak_B T \frac{\ln(g)}{\hbar g} + b \frac{\sqrt{\pi}}{2v_F} \left(\frac{k_B T}{\hbar} \right)^2 \frac{\ln(g)}{\sqrt{n}} + \text{const}, \quad (2)
 \end{aligned}$$

where $g(n)$ is the normalized conductivity defined as $g(n) = \sigma(n)h/e^2$ (σ : conductivity; h : Planck's constant). The first term corresponds to the inelastic scattering with a small momentum transfer. The direct Coulomb interaction, represented by the second term, corresponds to a large-momentum-transfer collision.^{13,14} This term, negligible near the base temperature of this study, shows a finite effect on the inelastic scattering at higher temperatures below ~ 20 K. This direct Coulomb interaction has not been considered for the inelastic scattering in previous works.^{2,3,5}

To compare the data with the prediction of Eq. (2), the inelastic-scattering rate (τ_ϕ^{-1}) is estimated from L_ϕ in Fig. 3(a) with the diffusion constant D obtained from the relations, $\sigma = (2e^2/h)k_F l$ and $D = v_F l/2$. Here, since n vanishes at the DP, we adopted the value of D at $V_{bg}=31$ V (just 1 V away from the DP) as its value of the DP. The resultant values of τ_ϕ^{-1} and the best fit with the *first term* in Eq. (2) are shown as filled circles and a solid line, respectively, in Fig. 3(b). The figure shows a nice fit for the gate voltages beyond ~ 15 V from the DP with $a \approx 10$ (for clarity, the data at DP are not shown in the figure). The growing discrepancy of the

observed τ_ϕ^{-1} from the fitting approaching the DP strongly suggests that additional inelastic scattering is present near the DP. As suggested in earlier studies,^{3,7} electron-hole puddles¹⁵ can be the cause of this behavior. Although the average carrier density vanishes near the DP, electrons and holes may form spatially fluctuating regions called puddles.¹⁵ In this circumstance, puddles can generate fluctuating electromagnetic field, which enhances the Nyquist scattering (large τ_N^{-1}). Thus, near the DP, charge carriers are supposed to be inelastically scattered more frequently than at gate voltages away from the DP, which can lead to additional phase breaking near the DP.

Figure 3(c) illustrates the temperature dependence of the inelastic (L_ϕ) and the elastic-scattering lengths (L_i and L_*) for the region of dense-electron carriers ($V_{bg}=60$ V). It is seen that the relation $L_\phi \gg L_i \geq L_*$ holds in almost the whole low-temperature range used in this study, where L_i and L_* turn out to be almost temperature independent. The inset of Fig. 3(d) shows the temperature dependence of L_ϕ at three gate voltages including the DP. In Figs. 3(c) and 3(d), L_ϕ increases with lowering temperature and is saturated at a certain value below a characteristic temperature T_{sat} , as marked in the inset of Fig. 3(d) by an arrow for each value of V_{bg} . The saturation of L_ϕ is simply expected with a finite concentration of magnetic impurities.¹⁷ However, as shown in the inset of Fig. 3(d), the value of T_{sat} depends on the carrier density (or V_{bg}). Since the amount of magnetic impurities should be independent of the carrier density, this behavior cannot be explained by the existence of magnetic impurities. As an alternative explanation of this saturation, one can resort to the formation of the electron-hole puddles¹⁵ again. By the presence of the electron-hole puddles, the effective conducting area for a charged carrier is reduced,¹⁵ which acts to limit the increase in L_ϕ . Approaching closer to the DP with a higher density of electron-hole puddles, the saturation of L_ϕ starts to take place at higher temperatures as shown in the inset of Fig. 3(d).

In Fig. 3(d), the inelastic-scattering rates τ_ϕ^{-1} at three gate voltages are shown as a function of temperature, where values of τ_ϕ^{-1} for $V_{bg}=60$ V (-35 V) is multiplied by a factor of three (ten) for clarity of the temperature dependence. As denoted by the solid lines in Fig. 3(d), data fit well to Eq. (2) at temperatures higher than T_{sat} . Nice fits are obtained only when the T^2 term in Eq. (2) is included, especially as V_{bg} deviates more from the DP. When we put Eq. (2) as $\tau_\phi^{-1} = \alpha T + \beta T^2$, the ratio β/α turns out to be about 0.016, 0.064, and 0.43 in an arbitrary unit for V_{bg} of 32 (the DP), 60, and -35 V, respectively. The ratio, a reference of the relative strength of the two terms in Eq. (2), indicates that the relative importance of the direct Coulomb interaction represented by the T^2 dependence of τ_ϕ^{-1} increases for a higher V_{bg} , although the absolute scattering rates of both of the two terms decrease.

In previous studies,^{2,3} data were fitted with the T -linear term only. Thus, the fit in Fig. 3(d) indicates that the direct Coulomb interaction is stronger in our graphene sheet. The direct Coulomb interaction involves a large-momentum

transfer,^{13,14} as in the elastic intervalley scattering denoted by the solid arrow in Fig. 1(c).⁹ This leads us to assuming that atomically sharp defects also cause the finite direct Coulomb interaction in our graphene sheet. Thus, in addition to the elastic intervalley scattering, it is probable that two charge carriers occupying states within the thermal energy difference of $k_B T$ in different valleys are scattered to each other in the vicinity of atomically sharp defects [the inset of Fig. 3(b)]. Interestingly, assuming that the scattering probability of a carrier in a valley is proportional to the number of available states to be scattered into in another valley, the cross section of this inelastic electron-electron intervalley scattering, a two-particle process, would have T^2 dependence. This is in accordance with the T^2 -dependence term in Eq. (2). The enhanced inelastic intervalley scattering in our sample, presumably with higher concentration of atomic-scale defects, also explains the difference of the WL behavior between this study and the previous ones.^{2,3} The existence of this inelastic-scattering mechanism may be further confirmed by separate experimental means, such as photoemission spectroscopy.

The saturation of the WL correction of the conductance may be caused as the phase coherence length L_ϕ becomes comparable to the sample length with lowering temperature.³ In our measurements, however, the saturation value of L_ϕ sensitively varies with V_{bg} and the saturation takes place for most range of V_{bg} in this study at temperatures far before L_ϕ reaches the sample length. At $V_{bg}=60$ V, for instance, where electron-hole puddles are barely present, L_ϕ is saturated at ~ 1.8 μm [see the inset of Fig. 3(d)]. This indicates that the finite-size effect is not the main cause of the saturation of L_ϕ .

IV. SUMMARY

In summary, we have measured the WL effect in graphene at various gate voltages (or alternatively carrier densities) and temperatures. The large chirality-breaking elastic intervalley scattering, presumably from atomically sharp defects,⁹ leads to relative characteristic length scales of $L_\phi \gg L_i \geq L_*$, which is in clear distinction from the conditions of previous works.²⁻⁵ It points that the transport properties in our graphene sheet may be more plagued by extrinsic characters. However, the chirality-breaking elastic intervalley scattering restores the conventional WL effect.^{3,10} The observed conventional WL characters in our graphene are solely dependent on the phase-breaking inelastic scattering¹¹ and thus provide a convenient condition to examine the inelastic-scattering properties in graphene.

In consequence, we could study the gate-voltage and temperature dependencies of the phase coherence length in detail, as shown in Fig. 3. Similar dependencies have also been observed in measurements of WL,^{3,6} UCF,^{6,7} and Aharonov-Bohm oscillation,⁸ but without the quantitative analysis. In this study, we show that the unusual gate-voltage and temperature dependencies of the phase coherence length are quantitatively explained in terms of the dominant inelastic electron-electron scattering^{13,14} while electron-hole puddles¹⁵ are expected to produce an additional inelastic scattering

near the DP.^{3,7} Different from previous works,^{2,3,5} the direct Coulomb interaction becomes effective at high temperatures of our study. We propose that it is caused by the large-momentum-transfer intervalley inelastic scattering in the vicinity of atomically sharp defects of charge carriers that occupy states within the thermal energy difference of $k_B T$ in different valleys.

ACKNOWLEDGMENTS

This work was supported by Acceleration Research (Grant No. R17-2008-007-01001-0) and Pure Basic Research (Grant No. R01-2006-000-11248-0) administered by Korea Science and Engineering Foundation, and by Korea Research Foundation (Grant No. KRF-2005-070-C00055).

*hjlee@postech.ac.kr

¹A. K. Geim and K. S. Novoselov, *Nat. Mater.* **6**, 183 (2007).

²S. V. Morozov, K. S. Novoselov, M. I. Katsnelson, F. Schedin, L. A. Ponomarenko, D. Jiang, and A. K. Geim, *Phys. Rev. Lett.* **97**, 016801 (2006).

³F. V. Tikhonenko, D. W. Horsell, R. V. Gorbachev, and A. K. Savchenko, *Phys. Rev. Lett.* **100**, 056802 (2008), and the supplementary document of this article.

⁴H. B. Heersche, P. Jarillo-Herrero, J. B. Oostinga, L. M. K. Vandersypen, and A. F. Morpurgo, *Nature (London)* **446**, 56 (2007).

⁵C. Berger, Z. Song, X. Li, X. Wu, N. Brown, C. Naud, D. Mayou, T. Li, J. Hass, A. N. Marchenkov, E. H. Conrad, P. N. First, and W. A. de Heer, *Science* **312**, 1191 (2006); X. Wu, X. Li, Z. Song, C. Berger, and W. A. de Heer, *Phys. Rev. Lett.* **98**, 136801 (2007).

⁶D. Graf, F. Molitor, T. Ihn, and K. Ensslin, *Phys. Rev. B* **75**, 245429 (2007). In this work, WL was also measured at various gate voltages but with a sheet consisting of several atomic layers.

⁷N. E. Staley, C. P. Puls, and Y. Liu, *Phys. Rev. B* **77**, 155429 (2008). This work was done in bilayer and trilayer graphite sheets instead of single-layer graphenes.

⁸S. Russo, J. B. Oostinga, D. Wehenkel, H. B. Heersche, S. S. Sobhani, L. M. K. Vandersypen, and A. F. Morpurgo, *Phys. Rev. B* **77**, 085413 (2008).

⁹H. Suzuura and T. Ando, *Phys. Rev. Lett.* **89**, 266603 (2002); T. Ando, *J. Phys. Soc. Jpn.* **73**, 1273 (2004); A. F. Morpurgo and F. Guinea, *Phys. Rev. Lett.* **97**, 196804 (2006).

¹⁰E. McCann, K. Kechedzhi, V. I. Fal'ko, H. Suzuura, T. Ando, and B. L. Altshuler, *Phys. Rev. Lett.* **97**, 146805 (2006); V. I. Fal'ko, K. Kechedzhi, E. McCann, B. L. Altshuler, H. Suzuura, and T. Ando, *Solid State Commun.* **143**, 33 (2007).

¹¹G. Bergmann, *Phys. Rep.* **107**, 1 (1984).

¹²J. C. Meyer, A. K. Geim, M. I. Katsnelson, K. S. Novoselov, T. J. Booth, and S. Roth, *Nature (London)* **446**, 60 (2007).

¹³M. J. Uren, R. A. Davies, M. Kaveh, and M. Pepper, *J. Phys. C* **14**, L395 (1981); B. L. Altshuler and A. G. Aronov, in *Electron-Electron Interaction in Disordered Systems*, edited by A. L. Efros and M. Pollak (Elsevier Science, Amsterdam, 1985).

¹⁴R. Taboryski and P. E. Lindelof, *Semicond. Sci. Technol.* **5**, 933 (1990); J. E. Hansen, R. Taboryski, and P. E. Lindelof, *Phys. Rev. B* **47**, 16040 (1993).

¹⁵J. Martin, N. Akerman, G. Ulbricht, T. Lohmann, J. H. Smet, K. Von Klitzing, and A. Yacoby, *Nat. Phys.* **4**, 144 (2008).

¹⁶J. González, F. Guinea, and M. A. H. Vozmediano, *Phys. Rev. Lett.* **77**, 3589 (1996); *Phys. Rev. B* **59**, R2474 (1999); S. Das Sarma, E. H. Hwang, and W.-K. Tse, *ibid.* **75**, 121406(R) (2007); M. Polini, R. Asgari, Y. Barlas, T. Pereg-Barnea, and A. H. MacDonald, *Solid State Commun.* **143**, 58 (2007).

¹⁷F. Pierre, A. B. Gougam, A. Anthore, H. Pothier, D. Esteve, and N. O. Birge, *Phys. Rev. B* **68**, 085413 (2003).